Stability of the Zhang-Rice Singlet with Doping in Lanthanum Strontium Copper Oxide Across the Superconducting Dome and Above

N. B. Brookes,[1,*] G. Ghiringhelli,[1,2] A.-M. Charvet,[3] A. Fujimori,[4] T. Kakeshita,[4] H. Eisaki,[5] S. Uchida,[4,5] and T. Mizokawa[6]

[1]European Synchrotron Radiation Facility, CS 40220, F-38043 Grenoble, Cedex 9, France
[2]Dipartimento di Fisica, Politecnico di Milano, Piazza Leonardo da Vinci 32, I-20133 Milano, Italy
[3]University Joseph Fourier, UGA, PhITEM, BP 53, F-38041 Grenoble, Cedex 9, France
[4]Department of Physics, University of Tokyo, Tokyo 113-0033, Japan
[5]National Institute of Advanced Industrial Science and Technology (AIST), Tsukuba 305-8568, Japan
[6]Department of Complexity Science and Engineering, University of Tokyo, Chiba 277-8561, Japan

(Received 30 July 2014; revised manuscript received 7 April 2015; published 7 July 2015)

The spin character of the states at the top of the valence band in doped $La_{2-x}Sr_xCuO_4$ ($x = 0.03$, 0.07, 0.15, 0.22, and 0.30) has been investigated using spin-polarized resonant photoemission. A clear Zhang-Rice singlet (ZRS) is observed at all doping levels. Its stability and polarization are preserved as a function of doping, suggesting that the concept of the ZRS can be used across a wide doping range and up to the metallic nonsuperconducting overdoped regime. The results are significant for theoretical models that use the ZRS approximation and for the understanding of the peculiar interplay between the ZRS and the remaining localized spins.

DOI: 10.1103/PhysRevLett.115.027002 PACS numbers: 74.25.Jb, 74.62.Dh, 74.72.-h, 79.60.-i

Understanding high-temperature superconductivity in the cuprates [1] is still one of the outstanding problems in solid state physics. Much progress has been made in determining the electronic structure of the parent compounds, which are found to be charge-transfer Mott insulators [2]. Some years ago, it was shown that the concept of Zhang-Rice singlets [3,4] was useful in describing the hole states in cuprates in the framework of the single-band Hubbard model [5] or the $t - J$ model [6–9]. The Zhang-Rice singlet (ZRS) is the two-hole state formed by pairing the spins of, respectively, a hole in the Cu $3d_{x^2-y^2}$ orbital and a hole distributed over the oxygen ligands in an antiparallel configuration. The existence of the ZRS was first demonstrated experimentally using spin-resolved resonant photoemission for CuO [10,11] and, subsequently, for optimally doped $Bi_2Sr_2CaCu_2O_{8+\delta}$ [12–14].

Although the ZRS model is often justified in the low doping limit, there is an on-going debate as to whether it is valid with increasing doping. Conflicting results have been obtained using oxygen K-edge x-ray absorption spectroscopy (XAS) [15–18]. A saturation of the intensity of the doping dependent XAS edge feature for a doping level above 0.21 was interpreted by Peets *et al.* [18] as a breakdown of the ZRS approximation, leading to the inapplicability of single-band Hubbard models in the overdoped regime. This generated significant debate [19–22] both in the interpretation of the data and the conclusions. Although similar saturation effects have also been reported in some photoemission experiments [15,23,24], recent XAS experiments [17] have shown that, up to a doping level of $x = 0.22$, there is no saturation of the intensity of the XAS feature, leading to the conclusion that the Zhang-Rice model is valid over the important doping regime covering the whole superconducting dome. As for theoretical aspects, some calculations of the oxygen K-edge XAS [25] led the authors to conclude to a failure of the entire three-band model, while others using large-scale exact diagonalization of the three-orbital Hubbard model [22], concluded that there is a continued relevance of the ZRS even in the overdoped regime. Theoretical work discussing resonant inelastic x-ray scattering (RIXS) results on magnetic excitations for doped cuprates [26] also suggests a possible failure of the ZRS picture away from the underdoped regime. There are suggestions of destabilization of the ZRS at optimum doping in the modeling of angle-resolved photoemission spectroscopy (ARPES) data [27], and others [28] have shown that there can be competing configurations for the lowest energy which might be preferred to the ZRS. Having more direct evidence for the breakdown or validity of the ZRS approximation is highly important for theoretical models describing the electronic structure and superconductivity in high-temperature superconductors [22,29] as well as for experimental work which often assumes its relevance [30,31].

The objective of the present experiment was to verify whether or not the ZRS concept could be applied to doped cuprates, from the underdoped to the overdoped compounds. Strontium doped lanthanum copper oxide was chosen because of the simplicity of the single copper oxide layer and the minimal structural changes with doping which allow samples to be compared across the series [32].

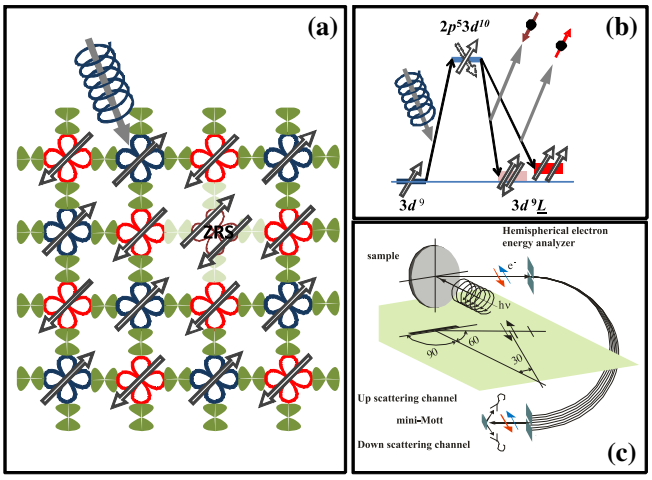

FIG. 1 (color online). (a) A schematic showing an antiferromagnetically ordered CuO plane. The energy and the circular polarization of the incident x-ray photons select undoped copper sites and their prevalent spin orientation, respectively. (b) A simplified energy diagram showing how singlet and triplet two-hole final states are distinguished by the spin of the photoemitted electron. (c) The experimental geometry for the spin-polarized resonant photoemission experiments [39].

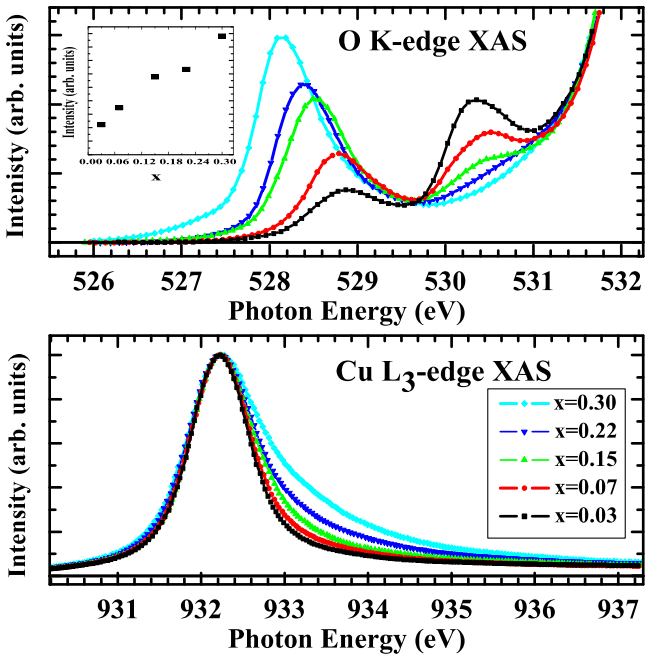

FIG. 2 (color online). The polarized ($E\perp c$) XAS of the O K edge and Cu L_3 edge of LSCO measured at low temperature as a function of doping x. The upper panel inset shows the maximum intensity of the lowest energy feature in the oxygen K-edge spectrum as a function of doping.

The basic assumption of our experiment is that the removal of one electron at the Fermi level by the photoelectric effect is equivalent to chemical doping [4]. Furthermore, by using resonant excitation, we can select Cu electronic states of initially undoped sites only [10,11], Fig. 1(a). This $3d^9$ copper site is chosen by tuning the energy of the x-rays to the L_3 peak in the absorption spectrum, Fig. 2. An electron is excited from the $2p_{3/2}$ spin-orbit split core states. In the intermediate state (i.e., $2p^53d^{10}$), the core hole preserves the memory of the $3d$ hole original spin direction, which has been selected by the sign of the circular polarization of the absorbed photon, Fig. 1(b). In this way, the intermediate state will decay via a $2p3d3d$ Auger process that restores the initial spin for one hole via the $3d$ to $2p$ transition and adds one extra $3d$ hole having spin either parallel or antiparallel to the initial one, therefore, leaving a triplet or singlet $2p^63d^8$ final state, respectively, Fig. 1(b). So, by measuring the spin polarization of the emitted electron, one can determine whether the two-hole final state is a triplet or singlet state. This $3d^8$ final state is hybridized with the two-hole state formed with a hole on the copper and surrounding oxygen sites (i.e., the ZRS state). The $3d^8$ contribution to the state is $<7\%$ but, due to the strong resonance ($\approx \times 100$), this allows one to probe the ZRS state. The two-hole final state produced in this way is equivalent to that produced by chemical doping [10]. The neighboring copper sites will be more or less doped depending on the sample doping level. Consequently, the experiment generates a doped site in the presence of other doped sites. By measuring a series of samples with increasing doping, one can determine how the electronic structure, including its spin character, changes with doping. The details of this method can be found in Refs. [10–14].

The $La_{2-x}Sr_xCuO_4$ ($x = 0.03$, 0.07, 0.15, 0.22, 0.3) (LSCO) single crystals were grown by the traveling-solvent floating-zone method and annealed so that the oxygen content became stoichiometric. The underdoped sample, $x = 0.03$, is insulating, those with $x = 0.07$, 0.15, and 0.22 are superconducting, and the overdoped sample, $x = 0.3$, is metallic without being superconducting. The growth details and sample characterization are described elsewhere [33–35]. The present results were obtained from the cleaved surfaces of crystals that were characterized by ARPES [36–38]. ARPES showed a systematic evolution of the Fermi surfaces up to the doping level of $x = 0.30$ demonstrating the high quality of the samples.

The $x = 0.3$ sample was cleaved with a cleaver at room temperature. The other samples were post-cleaved at low temperature. All samples were cleaved for each measurement and measured at a temperature <40 K. The experimental chamber pressure remained in the low 10^{-10} mbar range, and the samples showed no sign of degradation during the measurements. Each sample was measured several times during at least three separate experiments. The experiments were carried out at the ID8 helical undulator beam line of the European Synchrotron Radiation Facility, which provides almost 100% linear and circularly polarized light. The experimental geometry

is shown in Fig. 1(c). For the resonant photoemission measurements, the energy of the circularly polarized x-rays was tuned to the peak of the Cu $2p_{3/2}(L_3)$ photoabsorption white line ($h\nu \approx 932.2$ eV), Fig 2. The photon beam was at normal incidence to the sample, along the c axis of the crystal. The energy of the photoemitted electrons was analyzed using a hemispherical electron analyzer, with an angular acceptance of $\pm 20°$, mounted at a 60° angle relative to the incident light. The spin polarization of the energy resolved electrons was then analyzed using a mini-Mott spin detector [39]. The spin sensitivity of the detector is given by the Sherman function which was 0.17 at 25 keV electron scattering energy and was calibrated using the spin polarization of the ^1G peak from a CuO reference sample. The total energy resolution, including monochromator and analyzer, was ≈0.7 eV. To eliminate instrumental asymmetries, as well as the effect of possible drifts in the experimental setup, all spectra were collected with both light helicities and in alternating order. Any difference in detection efficiency between the two spin channels is, thus, eliminated.

The copper L-edge and oxygen K-edge XAS were measured in total electron yield at normal incidence, with linear polarized light and used to verify the quality and the reproducibility of the different cleaves. The energy resolution was 0.45 eV (0.16 eV) at the copper (oxygen) edge. Figure 2 shows the oxygen K-edge and Cu L_3-edge XAS for the five doping cases measured. As in a previous work [18], the spectra were normalized against each other using the energy ranges below and well above the main peak. The energy of the peaks was calibrated against earlier work [16]. A monotonic increase in the amplitude of the oxygen prepeak is seen as a function of doping, in agreement with C. T. Chen *et al.* [16]. However, the saturation in intensity for $x \geq 0.21$ reported by Peets *et al.* [18] is not observed with our samples, although the intensity increases more slowly than would be expected from a purely linear dependence [40]. This is consistent with recent results from Y.-J. Chen *et al.* [17]. Our measurements at the Cu L edges also show a monotonic increase of the shoulder above the edge with doping as in Ref. [16].

Figure 3(a) shows the valence band of LSCO ($x = 0.03$) measured at the Cu L_3 absorption maximum. The position of the Fermi level (E_F) was determined by measurements from a gold or silver foil in electrical contact with the sample. With the photon energy tuned at the Cu L_3 peak, the final state of the absorption process is dominated by the $2p^5 3d^{10}$ state. In Fig. 3(a), the main contributions to the spectrum come from the $3d^8$ final state with ^1S, ^1G, and ^3F character [10,11]. Figure 3(b) shows the spin polarization around the ^1G peak and the E_F region. The high spin polarization across the ^1G peak is consistent with its almost pure singlet character, which would give 83.3% spin polarization [10]. Likewise, the large spin polarization in the E_F region is indicative of a singlet state, a ZRS, as is

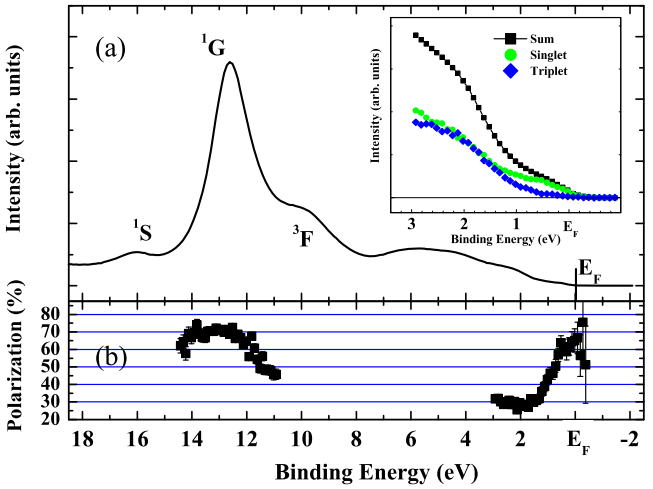

FIG. 3 (color online). (a) Spin-integrated circularly polarized L_3 resonant VB photoemission spectrum of LSCO for $x = 0.03$. (b) Spin polarization across the ^1G and E_F regions of the spectrum in the upper panel. The inset shows the spin-integrated VB photoemission spectrum close to the E_F as well as its singlet and triplet components derived using the spin polarization shown in the lower panel [41].

seen in other cuprates [10,12–14]. The inset in Fig. 3 shows the photoemission spectra in a 4 eV energy window close to E_F. Using the spin-polarization spectra, such as that shown in Fig. 3(b), together with the expected spin polarization for singlet and triplet final states, the spectral intensity is separated into the singlet and triplet contributions [42]. The state within 1.0 eV of the E_F is largely of singlet character and is separated from the triplet states by about 0.6 eV as shown in the inset of Fig. 3. In order to investigate the stability of the ZRS, we have measured the spin-polarized spectra in the E_F region for $x = 0.03, 0.07, 0.15, 0.22, 0.3$. The upper panel of Fig. 4 shows the spin-integrated intensity close to E_F for the five cases. The results shown in Fig. 4 are all coming from data taken during the same experimental run. Data taken in different runs or cleaves give consistent results within the error bars. The intensity was normalized to 100% at 2.34 eV binding energy for all curves. The shape of the structure close to E_F and the degree of polarization are similar in all cases. For a more precise comparison, each spectrum is divided into three regions: the plateau close to the E_F, where the intensity of the singlet state is dominant (polarization ≈ 60%), a sloping region where mixing between the singlet and the triplet state occurs, and a lower plateau where singlet and triplet states have similar intensities (polarization ≈30%) as shown in Fig. 3. The limits of these three regions are characterized by points A and B, which are shown as arrows for the case $x = 0.03$ in Fig. 4. Figure 5 shows the binding energies corresponding to points A and B for each doping level. Averaging over x, the binding energies are, respectively, 0.60 ± 0.09 eV for point A and 1.48 ± 0.09 eV for point B. To the precision of our measurements, all samples

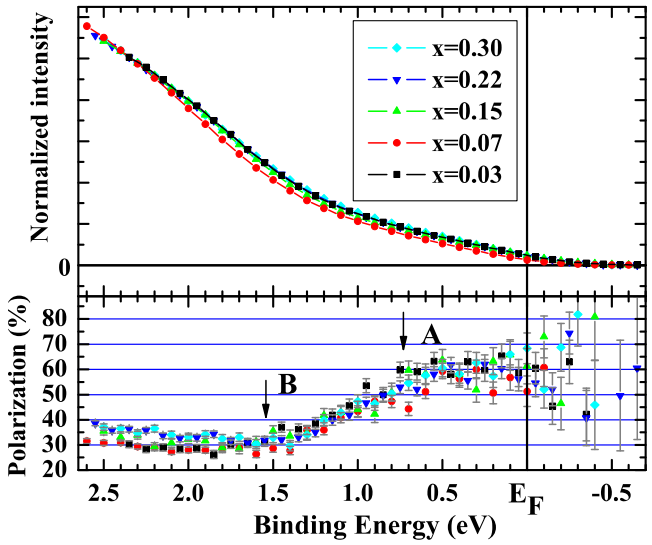

FIG. 4 (color online). Upper panel: Spin-integrated circularly polarized L_3 resonant VB photoemission spectrum of LSCO. The lower panel shows the corresponding spin-polarization spectra. Points A and B are defined in the text.

have the same binding energies for characteristic points A and B. Point A is of particular significance, because it corresponds to the bottom of the triplet states below which the near E_F states are dominated by the singlet. The energy spacing between point A and the E_F is seen in Fig. 5 to be $\approx$0.6 eV, meaning that the separation between the triplet and singlet states is at least 0.6 eV, a significant value. Point B defines the start of the region over which the singlet and the triplet states are almost equally mixed. Figure 5 also shows the data corresponding to the spin polarization

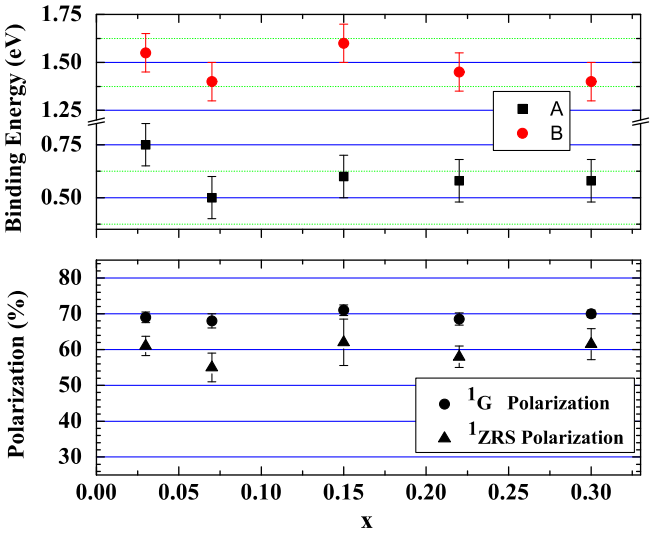

FIG. 5 (color online). Upper panel: Binding energies of characteristic points A (filled square) and B (filled circle) from Fig. 4 as a function of doping x. Lower panel: Polarization of ^1G and of the ZRS as a function of doping.

averaged over an energy window of 0.6 eV just below E_F, which we expect to represent the singlet state. The corresponding spin polarization of both the ^1G and the ZRS peaks are essentially constant with doping, and this serves as an internal check of data consistency.

The present Letter contributes significantly to the long standing debate on the robustness of the ZRS against doping as it directly probes the presence of singlet states by measuring their spin polarization. The measured degree of spin polarization is evidence that the state close to E_F is mostly of singlet character. Also, as a function of doping, the data show little change in the spin polarization close to E_F and the triplet-singlet energy separation is essentially unchanged. Therefore, our results indicate that there exists a singlet state stable with doping, providing the first direct evidence that, for LSCO, the ZRS model is valid for the entire region of doping where the superconducting dome exists. Indeed, we show that, even for $x = 0.3$ (where the sample is no longer superconducting), there is not a sufficient modification of the underlying electronic structure to destroy the singlet state close to E_F. This conclusion is of general importance since the ZRS concept is used for the interpretation of experimental results as well as for theoretical models used to describe the electronic properties of the cuprates. As discussed in Ref. [22], several theoretical models remain consistent with the results presented here, either the single-band Hubbard model implemented by cluster dynamical mean-field theory calculations, or a three-orbital Hubbard model implemented through large-scale exact diagonalization. Interestingly, our findings are consistent with a recent RIXS study [43] which shows that magnetic excitations persist across the entire doping range considered here. This means that, since the top of the VB is dominated by the ZRS even in the overdoped regime, most of the doped holes locally form the ZRS with the Cu spins, and the remaining Cu spins can still sustain the magnetic excitations observed up to the overdoped regime.

We would like to thank K. Larsson for his invaluable support and L. H. Tjeng and T. P. Devereaux for stimulating discussions.

*Corresponding author.
brookes@esrf.fr

[1] J. G. Bednorz and K. A. Muller, Z. Phys. B **64**, 189 (1986).
[2] J. Zaanen, G. A. Sawatzky, and J. W. Allen, Phys. Rev. Lett. **55**, 418 (1985).
[3] F. C. Zhang and T. M. Rice, Phys. Rev. B **37**, 3759 (1988).
[4] H. Eskes and G. A. Sawatzky, Phys. Rev. Lett. **61**, 1415 (1988).
[5] P. W. Anderson, Science **235**, 1196 (1987).
[6] E. Dagotto, Rev. Mod. Phys. **66**, 763 (1994).
[7] E. W. Carlson, S. A. Kivelson, Z. Nussinov, and V. J. Emery, Phys. Rev. B **57**, 14704 (1998).
[8] T. Tohyama, C. Gazza, C. T. Shih, Y. C. Chen, T. K. Lee, S. Maekawa, and E. Dagotto, Phys. Rev. B **59**, R11649 (1999).

[9] S. R. White and D. J. Scalapino, Phys. Rev. B **61**, 6320 (2000).
[10] L. H. Tjeng, B. Sinkovic, N. B. Brookes, J. B. Goedkoop, R. Hesper, E. Pellegrin, F. M. F. de Groot, S. Altieri, S. L. Hulbert, E. Shekel, and G. A. Sawatzky, Phys. Rev. Lett. **78**, 1126 (1997).
[11] L. H. Tjeng, N. B. Brookes, and B. Sinkovic, J. Electron Spectrosc. Relat. Phenom. **117–118**, 189 (2001).
[12] N. B. Brookes, G. Ghiringhelli, O. Tjernberg, L. H. Tjeng, T. Mizokawa, T. W. Li, and A. A. Menovsky, Phys. Rev. Lett. **87**, 237003 (2001).
[13] G. Ghiringhelli, N. B. Brookes, L. H. Tjeng, T. Mizokawa, O. Tjernberg, P. G. Steeneken, and A. A. Menovsky, Physica (Amsterdam) **312–313B**, 34 (2002).
[14] G. Ghiringhelli, Ph.D. thesis, Université Joseph Fourier—Grenoble I, 2002.
[15] M. Schneider, R.-S. Unger, R. Mitdank, R. Muller, A. Krapf, S. Rogaschewski, H. Dwelk, C. Janowitz, and R. Manzke, Phys. Rev. B **72**, 014504 (2005).
[16] C. T. Chen, L. H. Tjeng, J. Kwo, H. L. Kao, P. Rudolf, F. Sette, and R. M. Fleming, Phys. Rev. Lett. **68**, 2543 (1992).
[17] Y.-J. Chen, M. G. Jiang, C. W. Luo, J.-Y. Lin, K. H. Wu, J. M. Lee, J. M. Chen, Y. K. Kuo, J. Y. Juang, and Chung-Yu Mou, Phys. Rev. B **88**, 134525 (2013).
[18] D. C. Peets, D. G. Hawthorn, K. M. Shen, Y.-J. Kim, D. S. Ellis, H. Zhang, S. Komiya, Y. Ando, G. A. Sawatzky, R. Liang, D. A. Bonn, and W. N. Hardy, Phys. Rev. Lett. **103**, 087402 (2009).
[19] P. Phillips and M. Jarrell, Phys. Rev. Lett. **105**, 199701 (2010).
[20] D. C. Peets, D. G. Hawthorn, K. M. Shen, G. A. Sawatzky, R. Liang, D. A. Bonn, and W. N. Hardy, Phys. Rev. Lett. **105**, 199702 (2010).
[21] A. Liebsch, Phys. Rev. B **81**, 235133 (2010).
[22] C.-C Chen, M. Sentef, Y. F. Kung, C. J. Jia, R. Thomale, B. Moritz, A. P. Kampf, and T. P. Devereaux, Phys. Rev. B **87**, 165144 (2013).
[23] A. Ino, T. Mizokawa, K. Kobayashi, A. Fujimori, T. Sasagawa, T. Kimura, K. Kishio, K. Tamasaku, H. Eisaki, and S. Uchida, Phys. Rev. Lett. **81**, 2124 (1998).
[24] T. Yoshida, X. J. Zhou, H. Yagi, D. H. Lu, K. Tanaka, A. Fujimori, Z. Hussain, Z.-X. Shen, T. Kakeshita, H. Eisaki, S. Uchida, K. Segawa, A. N. Lavrov, and Y. Ando, Physica (Amsterdam) **351B**, 250 (2004).
[25] X. Wang, L. de'Medici, and A. J. Millis, Phys. Rev. B **81**, 094522 (2010).
[26] W. Chen and O. P. Sushkov, Phys. Rev. B **88**, 184501 (2013).
[27] D. K. Sunko, J. Exp. Theor. Phys., **109**, 652 (2009).
[28] L. Hozoi, S. Nishimoto, and A. Yamasaki, Phys. Rev. B **72**, 144510 (2005).
[29] T. Morinari, J. Phys. Soc. Jpn. **81**, 074716 (2012).
[30] D. Meyers, S. Mukherjee, J.-G. Cheng, S. Middey, J.-S. Zhou, J. B. Goodenough, B. A. Gray, J. W. Freeland, T. Saha-Dasgupta, and J. Chakhalian, Sci. Rep. **3**, 1834 (2013).
[31] N. Hollmann, Z. Hu, A. Maignan, A. Günther, L.-Y. Jang, A. Tanaka, H.-J. Lin, C. T. Chen, P. Thalmeier, and L. H. Tjeng, Phys. Rev. B **87**, 155122 (2013).
[32] B. Keimer, N. Belk, R. J. Birgeneau, A. Cassanho, C. Y. Chen, M. Greven, M. A. Kastner, A. Aharony, Y. Endoh, R. W. Erwin, and G. Shirane, Phys. Rev. B **46**, 14034 (1992).
[33] K. Tamasaku, Y. Nakamura, and S. Uchida, Phys. Rev. Lett. **69**, 1455 (1992).
[34] Y. Nakamura and S. Uchida, Phys. Rev. B **47**, 8369 (1993).
[35] S. Uchida, K. Tamasaku, and S. Tajima, Phys. Rev. B **53**, 14558 (1996).
[36] A. Ino, C. Kim, M. Nakamura, T. Yoshida, T. Mizokawa, Z.-X. Shen, A. Fujimori, T. Kakeshita, H. Eisaki, and S. Uchida, Phys. Rev. B **62**, 4137 (2000).
[37] A. Ino, C. Kim, M. Nakamura, T. Yoshida, T. Mizokawa, A. Fujimori, Z.-X. Shen, T. Kakeshita, H. Eisaki, and S. Uchida, Phys. Rev. B **65**, 094504 (2002).
[38] T. Yoshida, X. J. Zhou, M. Nakamura, S. A. Kellar, P. V. Bogdanov, E. D. Lu, A. Lanzara, Z. Hussain, A. Ino, T. Mizokawa, A. Fujimori, H. Eisaki, C. Kim, Z.-X. Shen, T. Kakeshita, and S. Uchida, Phys. Rev. B **63**, 220501(R) (2001).
[39] G. Ghiringhelli, K. Larsson, and N. B. Brookes, Rev. Sci. Instrum. **70**, 4225 (1999).
[40] A similar trend is observed whether one plots the maximum intensity of the lower energy feature or an integrated intensity over a fixed energy window encompassing this first feature.
[41] The error bars are calculated as described in J. Kessler, *Polarized Electrons* (Springer-Verlag, Berlin, 1976). Details can be found in Ref. [14].
[42] Assuming that a pure singlet (triplet) state has $5/6$ ($-5/18$) polarization, the singlet and triplet intensities are simply retrieved from the total intensity (I) and the spin polarization(P) as $I_{\text{singlet}} = (I/4)[1 + 3P/(5/6)]$ and $I_{\text{triplet}} = (I/4)[3 - 3P/(5/6)]$. Then $I = I_{\text{singlet}} + I_{\text{triplet}}$, and if the polarization is $5/6$ ($-5/18$), one has a pure singlet (triplet) state.
[43] M. P. M. Dean, G. Dellea, R. S. Springell, F. Yakhou-Harris, K. Kummer, N. B. Brookes, X. Liu, Y-J. Sun, J. Strle, T. Schmitt, L. Braicovich, G. Ghiringhelli, I. Božović, and J. P. Hill, Nat. Mater. **12**, 1019 (2013).